NANO LETTERS

2007
Vol. 7, No. 6
1676−1679

Optical Properties of a Wrinkled Nanomembrane with Embedded Quantum Well

Yongfeng Mei,*,†,‡ Suwit Kiravittaya,† Mohamed Benyoucef,† Dominic J. Thurmer,† Tim Zander,† Christoph Deneke,† Francesca Cavallo,† Armando Rastelli,†,‡ and Oliver G. Schmidt§

Max-Planck-Institut für Festkörperforschung, Heisenbergstrasse 1, D-70569 Stuttgart, Germany, and Institute for Integrative Nanosciences, IFW Dresden, Helmholtzstrasse 20, D-01069 Dresden, Germany

Received March 20, 2007; Revised Manuscript Received April 17, 2007

ABSTRACT

A wrinkled nanomembrane with embedded quantum well (QW), fabricated by the partial release and bond back of epitaxial layers upon underetching, is investigated by spatially resolved micro-photoluminescence spectroscopy. From the observed QW transition energies and calculations based on the linear deformation potential theory, we find that the bonded back regions are fully relaxed and act on the strain state of the wrinkled QW. Light emission enhancement observed in the wrinkled QW is explained by interference contrast theory.

The deterministic release and rearrangement of thin solid films or nanomembranes on substrate surfaces[1] offers exciting possibilities toward advanced integration strategies on a single chip, such as folded and rolled-up nanotechnology,[2,3] micro- and nano-origami,[4] stretchable electronics,[5,6] and thin membrane transfer.[7] These technologies might lead to hybrid material heterostructure and superlattice systems[8,9] with interdisciplinary functionalities in electronics,[2,5−7] X-ray,[10] infrared,[11,12] and visible optics,[13] as well as nanomechanics[14] and nanofluidity.[15,16]

Very recently, it has been shown that the partial release and bond back of layers (REBOLA) can be used to create complex nanochannel networks on substrate surfaces by deterministic wrinkling.[17] For the evolution of wrinkling, different relaxation behaviors have been studied to understand various patterns and their transitions.[18−21] However, there has been little work elucidating the electronic or optical properties of such wrinkled membranes.

In this Letter, we embed a strained quantum well (QW) layer into a semiconductor heterostructure and create a wrinkled nanomembrane on a substrate surface by the REBOLA technique. The optical properties of such a wrinkled QW layer are experimentally recorded by spatially resolved micro-photoluminescence (μ-PL) spectroscopy and theoretically determined by linear deformation potential theory. A comparison between experiment and theory allows us to determine the strain state in the wrinkled and bonded back layer. Furthermore, we find that the PL emission intensity is enhanced in wrinkled areas, which we can explain by interference contrast theory.

The sample structure (AlAs/GaAs/InGaAs/GaAs) sketched in Figure 1a is grown on a semi-insulating GaAs (001) substrate by solid-source molecular beam epitaxy. After deoxidation of the substrate in ultrahigh vacuum, a 400 nm thick GaAs buffer is grown followed by a sacrificial layer of 80 nm AlAs. The wrinkling layer consists of a nominally 4 nm thick $In_{0.22}Ga_{0.78}As$ QW layer sandwiched between two 10 nm thick GaAs barrier layers. The GaAs buffer is grown at 580 °C and the AlAs/GaAs/$In_{0.22}Ga_{0.78}As$/GaAs layer structure is deposited at 450 °C. Patterns on the sample surface are prepared by photolithography followed by reactive ion etching using $SiCl_4$ gas or wet chemical etching in a HBr solution.[22] The AlAs sacrificial layer of the sample is selectively removed by a 3−5 min etching with a diluted HF (∼0.06%) solution. For μ-PL measurements, the sample is mounted on the coldfinger of a He flow cryostat that can be moved by computer-controlled *xy*-linear translation stages with a spatial resolution of 50 nm. The measurement is performed at a sample temperature of 6 K using a frequency-doubled Nd:YVO_4-laser operating at 532 nm as excitation source. The laser is focused by a microscope objective (with numerical aperture = 0.6) to a spot diameter of roughly 1 μm. The same microscope objective is used to collect the PL emission. The luminescence is then spectrally filtered

* Corresponding author: y.mei@ifw-dresden.de.
† Max-Planck-Institut für Festkörperforschung.
‡ Present address: Institute for Integrative Nanosciences, IFW Dresden.
§ Institute for Integrative Nanosciences, IFW Dresden.

10.1021/nl070653e CCC: $37.00
Published on Web 04/27/2007

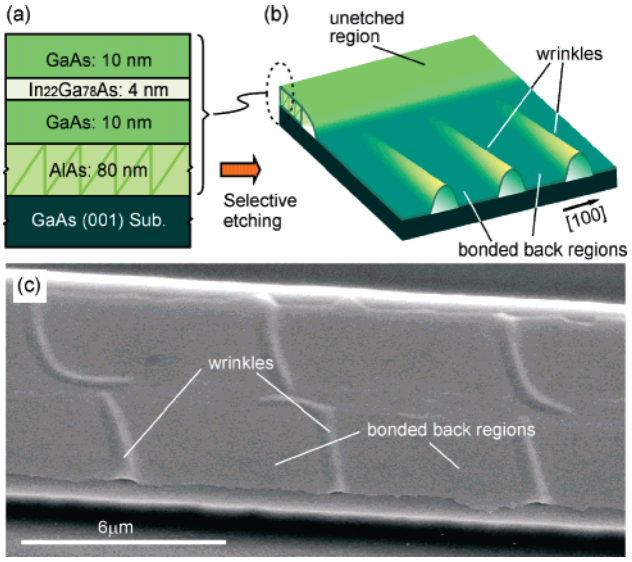

Figure 1. Schematic diagrams of (a) An as-grown structure containing a QW layer and (b) A wrinkled nanomembrane structure. (c) A scanning electron microscopy image of the wrinkled QW.

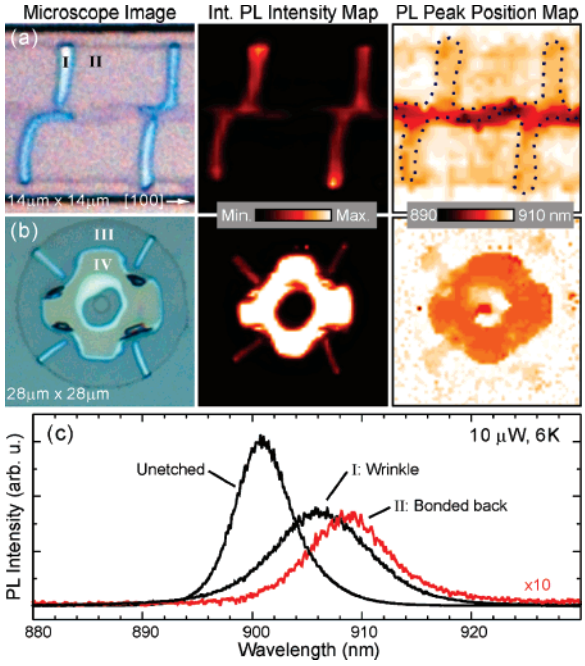

Figure 2. (a and b) Optical microscopy images, integrated PL intensity maps, and PL peak position maps (from left to right) of a QW in linear (I, wrinkle; II, bonded back region) and circular (III, etched region; IV, unetched region) channel networks, respectively. (c) PL spectra of unetched QW layer, wrinkled QW, and bonded back QW.

by a 750 mm focal length spectrometer equipped with a liquid-N_2-cooled Si charge-coupled-device.

A sketch of the wrinkled nanomembrane with micro-/nanochannel structures, fabricated by REBOLA method, is displayed in Figure 1b. Ordered wrinkles are formed perpendicularly to the etching front. The etching depth and the shape of the starting window influence the formation, size, and shape of the wrinkle. A typical structure is shown in Figure 1c. After deterministic wrinkling and bond back, the etched layer is characterized by two types of regions: wrinkles (I) and bonded back layer (II). The wrinkles experience an arc shape, are 900−1000 nm wide, and around 120 nm high at the open end. The channel height gradually decreases toward the unetched region. The average wrinkle periodicity is around 8 μm. The wrinkles form due to the relaxation of the compressively strained QW upon release of the layer. The size and geometry of the wrinkles can be controlled by several experimental parameters such as surface patterning and etching conditions.[17]

Parts a and b of Figure 2 show linear and circular wrinkling geometries, respectively. The left panels display optical microscopy images, while the middle and right panels show maps of integrated PL intensity and PL peak position, respectively. The circular structure is obtained by underetching a ringlike mesa (III, etched region; IV, unetched region). From the intensity maps we see that the PL intensity from the wrinkled regions is stronger than that from the bonded back regions, while the peak position maps show that the emission from the wrinkles is slightly blue-shifted compared to the emission from bonded back regions. In Figure 2c, representative PL spectra collected from a wrinkle (I) and from a bonded back region (II) are shown together with a spectrum from an unetched region. Because of the extra surface created during etching and associated nonradiative recombination centers, the integrated PL intensity from the wrinkles and bonded back regions drops compared to the unetched regions (see also middle panel of Figure 2b). The intensity from the wrinkled regions is about 10 times higher than the intensity from the bonded back regions. Moreover, the emission from the underetched regions is strongly red-shifted with respect to the unetched regions, with the bonded back regions displaying the longest wavelength. From the Gaussian fits of the PL peaks, peak energy values of 1.3762, 1.3644, and 1.3684 eV are extracted for the unetched, the bonded back, and the wrinkled QW, respectively.

The shift of the QW emission peak position can be used to monitor the strain state in the layer after deformation since the strain affects the electronic structure of the QW layer. Assuming different strain states for each structure, we can deduce the residual stresses and the lattice constants as shown schematically in Figure 3a. Since our as-grown InGaAs QW has a thickness below the critical value for dislocation introduction, the compressive strain is fully confined in the QW layer. After the removal of the sacrificial layer (AlAs) by selective etching, the strain of the QW layer in the bonded back region is partially relaxed due to the release of the sandwiched QW layer. In this case the equilibrium configuration is between the fully strained QW (without tensile strain in the barrier layers) and fully relaxed QW (with high tensile strain in the barrier layers). In order to calculate the residual strain in each layer, we perform a strain energy minimization of the structure.[25,26] This results in tensile strain (0.237%) in the barrier layers due to the partial relaxation of the compressive strain in the QW. A schematic of the forces and lattice constants after relaxation is shown in the middle panel of Figure 3a. For the wrinkled region, the bending of the film produces a inhomogeneous strain distribution where the lattice constant along the growth

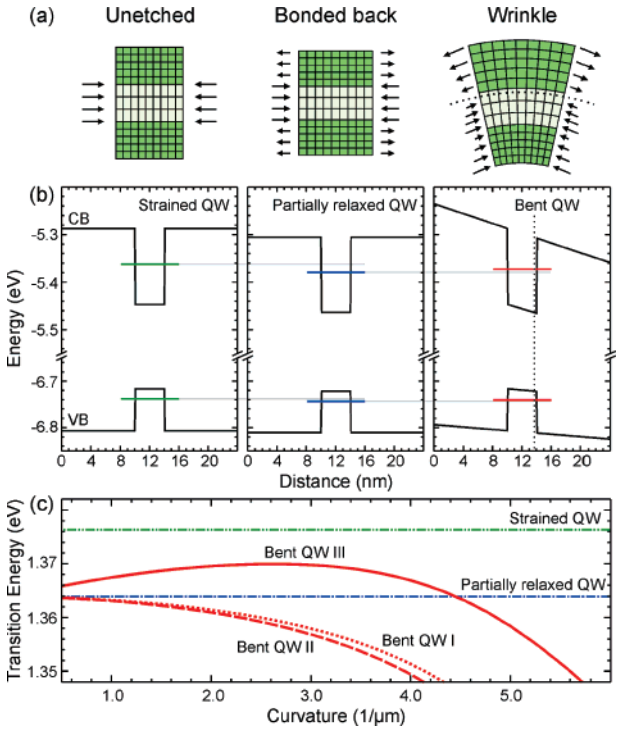

Figure 3. (a) Schematic of the unetched (strained QW), bonded back (partially relaxed QW), and wrinkle (bent QW) structures. Arrows represent the force applied to the layer, and the dotted line in the wrinkle structure indicates the neutral plane. (b) Band diagram corresponding to the structure shown in (a). The lines in the middle of the QW show the quantized energy levels of the electron in conduction band (CB) and heavy hole in the valence band (VB). Light-gray lines are guides to the eyes. (c) Transition energy of the bent QW as a function of the bending curvature. The dashed-dotted−dotted and the dashed-dotted lines represent the transition energy of the strained QW and partially relaxed QW, respectively. Three bent QW models are presented (see text for details).

direction is a function of inner lattice constant and the curvature and is varied linearly with the distance from the inner wrinkle surface (see eq 1 in ref 26). Assuming a certain position for the neutral plane, defined as the plane where there is no change of the strain state before and after bending[23] (dotted line), we can obtain the residual forces, which can be tensile or compressive as shown in the right panel of Figure 3a. By applying linear deformation potential theory,[27] we can draw the corresponding band diagrams as well as numerically calculate the quantized energy levels of these QW structures as shown in Figure 3b. For the strained QW, we obtain a transition energy of 1.3762 eV when we assume an indium content of 0.218 for the 4 nm thick QW.[24] The strain relaxation of this QW is calculated by minimizing the total strain energy of the structure.[25] The relaxation leads to a smaller transition energy of 1.3638 eV for the partially relaxed QW in the released layer. This value (12.4 meV lower than the strained QW) agrees well with the experimental observation (11.8 meV). For the bent QW, we have to assume that the neutral plane (dotted line) lies ~1.7 nm above the center of the QW in order to obtain a reasonable fit with the experiment (see discussion below). The schematic of the bent QW is shown on the right panel of Figure 3b. From this calculation, we obtain a transition energy of 1.3683 eV for a curvature of 1.33 μm^{-1}, which is extracted from the atomic force microscopy (AFM) height profile of the wrinkle.

Figure 3c summarizes the calculation of the transition energy as a function of curvature. In this plot, the transition energies for the strained and partially relaxed QWs are also shown as horizontal dashed-dotted lines for reference. For the bent QW (wrinkle), we consider three models in order to understand the experimental result. In the first model (Bent QW I), the minimization of the strain energy in polar coordinates is performed at a fixed curvature. The tangential lattice constant is extracted from the minimum energy configuration.[26] The result (dotted line in Figure 3c) indicates *only* a red shift of the transition energy as compared to the partially relaxed QW, in contradiction with the experimental observation. For the second model (Bent QW II), based on the fact that the grown structure is symmetric, we assume the neutral plane at the center of the QW. The calculation also shows only a red shift, which cannot fit the experimental result. For the third model (Bent QW III), the position of the neutral plane is varied as a fitting parameter. In this case we can obtain a blue shift of the PL energy (4−6 meV) with respect to the partially relaxed QW within the curvature range of 1−2 μm^{-1}. Note that in all three models the transition energy approaches the value for the partially relaxed QW when the curvature approaches zero (very large radius = flat surface). For the last model (Bent QW III), a red shift is observed for large curvatures (small radii), which we do not expect in the presented structures. From this calculation, we conclude that the wrinkle structure is in a nonequilibrium strain state for our geometry without any external force. This might originate from the fact that the nearby bonded back film influences the strain state of the wrinkle.

The wrinkled structures display a stronger PL emission intensity compared to that of the bonded back regions (see Figure 2c). In order to quantify this effect, we investigate another large wrinkle (its height is about 160 nm at the open end). As shown in Figure 4a, its integrated PL intensity map reveals two maxima across the high part of the wrinkle and only a single maximum in the regions with reduced height.

On the basis of the geometry of our structure and on the measurement setup, several effects are considered in order to calculate the relative PL intensity I as a function of measurement position. These effects are (i) interference−enhancement,[28] (ii) effective excited area due to wrinkling, and (iii) power distribution of the excitation laser spot. I can be expressed as

$$I(x_0,y_0) \propto \int\int F(h)\, R(S/S_0)\cdot P(x-x_0,y-y_0)\, dx\, dy \quad (1)$$

where (x_0,y_0) represents the measurement position; F is the interference factor, which is a function of the height h of the emitter from the "mirror" surface; R is the ratio of the effective excited area S of a wrinkled region over the corresponding flat region S_0; and P is the power distribution across the excitation laser spot. On the basis of interference−contrast theory,[28] an enhanced signal can be obtained when the active structure is above the substrate, because of the

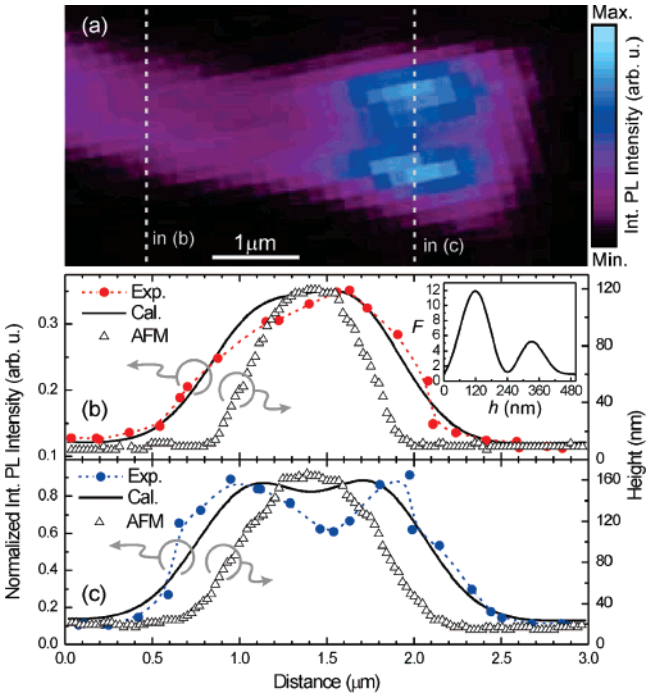

Figure 4. (a) Integrated PL intensity mapping of a large wrinkle. (b and c) AFM height profiles, integrated PL intensities, calculated PL relative intensities as a function of the position in the wrinkles either in the higher and lower ends of the wrinkle (dashed lines in (a)).

interference between the reflected light from the substrate and the direct light from the emitter. The calculation based on this theory is shown in the inset of Figure 4b. The interference factor F is plotted as a function of h. (Realistic material parameters at the corresponding excitation and emission wavelengths are taken from ref 29.) By calculating R from the AFM height curves shown in parts b and c of Figure 4 and assuming a Gaussian distribution with a full width at half-maximum (fwhm) of 0.625 μm for the laser power P, we can calculate the intensity curves from eq 1 and compare them to the experimental data. Our calculation agrees well with the experimental data as shown in parts b and c of Figure 4. The deviation may be due to the limited spatial resolution of the PL setup.

In summary, a wrinkled nanomembrane with embedded QW is fabricated by the REBOLA method and its optical properties are spatially resolved by μ-PL spectroscopy. The wrinkled layer deformation after deterministic wrinkling and bond-back is revealed by the shifts of the transition energies of embedded QWs together with detailed quantized energy calculations, which include the effect of strain relaxations. We find that the neutral plane of the wrinkle is shifted away from the equilibrium state while the layer in the bonded back regions is fully relaxed. Light emission enhancement of the wrinkled QW is attributed to interference effects, which agrees well with a numerical calculation. Our experimental findings and theoretical calculations present an understanding of the optical properties of wrinkled QWs, which might act as functional layers for read out and detection in highly integrative nanochannel networks on a single chip.[17]

Acknowledgment. We thank Dr. M. Stoffel, Dr. A. Malachias, Dr. R. Costescu, and L. Wang for helpful discussions as well as E. Coric, A. Schulz, W. Winter, and M. Riek for experimental assistance. This work is financially supported by the BMBF (03N8711).

References

(1) Schmidt, O. G.; Schmarje, N.; Deneke, C.; Muller, C.; Jin-Phillipp, N. Y. *Adv. Mater.* **2001**, *13*, 756.
(2) Schmidt, O. G.; Eberl, K. *Nature* **2001**, *410*, 168.
(3) Prinz, V. Ya.; Seleznev, V. A.; Gutakovsky, A. K.; Chehovsky, A. V.; Preobrazhenski, V.; Putyato, M. A.; Gavrilova, T. A. *Physica E* **2000**, *6*, 828.
(4) Vaccaro, P. O.; Kubota, K.; Aida, T. *Appl. Phys. Lett.* **2001**, *78*, 2825.
(5) Khang, D.-Y.; Jiang, H.; Huang, Y.; Rogers, J. A. *Science* **2006**, *311*, 208.
(6) Sun, Y.; Kumar, V.; Adesida, I.; Rogers, J. A. *Adv. Mater.* **2006**, *18*, 2857.
(7) Roberts, M. M.; Klein, L. J.; Savage, D. E.; Slinker, K. A.; Friesen, M.; Celler, G.; Eriksson, M. A.; Lagally, M. G. *Nat. Mater.* **2006**, *5*, 388.
(8) Deneke, Ch.; Jin-Phillipp, N.-Y.; Loa, I.; Schmidt, O. G. *Appl. Phys. Lett.* **2004**, *84*, 4475.
(9) Deneke, Ch.; Zschieschang, U.; Klauk, H.; Schmidt, O. G. *Appl. Phys. Lett.* **2006**, *89*, 263110.
(10) Deneke, Ch.; Schmidt, O. G. *Appl. Phys. Lett.* **2006**, *89*, 123121.
(11) Mendach, S.; Songmuang, R.; Kiravittaya, S.; Rastelli, A.; Benyoucef, M.; Schmidt, O. G. *Appl. Phys. Lett.* **2006**, *88*, 111120.
(12) Kipp, T.; Welsch, H.; Strelow, C.; Heyn, C.; Heitmann, D. *Phys. Rev. Lett.* **2006**, *96*, 077403.
(13) Songmuang, R.; Rastelli, A.; Mendach, S.; Schmidt, O. G. *Appl. Phys. Lett.* **2007**, *90*, 091905.
(14) Zhang, L.; Ruh, E.; Grützmacher, D.; Dong, L.; Bell, D. J.; Nelson, B. J.; Schönenberger, C. *Nano Lett.* **2006**, *6*, 1311.
(15) Deneke, Ch.; Schmidt, O. G. *Appl. Phys. Lett.* **2004**, *85*, 2914.
(16) Thurmer, D. J.; Deneke, C.; Mei, Y. F.; Schmidt, O. G. *Appl. Phys. Lett.* **2006**, *89*, 223507.
(17) Mei, Y. F.; Thurmer, D. J.; Cavallo, F.; Kiravittaya, S.; Schmidt, O. G. *Adv. Mater.*, in press. (It can be reached at http://arxiv.org/abs/cond-mat/0612602).
(18) Mutz, M.; Bensimon, D.; Brienne, M. J. *Phys. Rev. Lett.* **1991**, *67*, 923.
(19) Yoo, P. J.; Lee, H. H. *Phys. Rev. Lett.* **2003**, *91*, 154502.
(20) Huang, Z.; Hong, W.; Suo, Z. *Phys. Rev. E* **2004**, *70*, 030601.
(21) Chaieb, S.; Natrajan, V. K.; El-rahman, A. A. *Phys. Rev. Lett.* **2006**, *96*, 078101.
(22) Rastelli, A.; Ulhaq, A.; Deneke, Ch.; Wang, L.; Benyoucef, M.; Coric, E.; Winter, W.; Mendach, S.; Horton, F.; Cavallo, F.; Merdzhanova, T.; Kiravittaya, S.; Schmidt, O. G. *Phys. Status Solidi C* **2006**, *3*, 3641.
(23) Landau, L. D.; Lifshitz, L. *Theory of Elasticity*, 3rd ed.; Pergamon: New York, 1986.
(24) The exciton binding energy, which is approximately constant for this calculation, is neglected.
(25) Pryor, C.; Pistol, M-E.; Samuelson, L. *Phys. Rev. B* **1997**, *56*, 10404.
(26) Grundmann, M. *Appl. Phys. Lett.* **2003**, *83*, 2444.
(27) Van de Walle, C. G. *Phys. Rev. B* **1989**, *39*, 1871.
(28) Lambacher, A.; Fromherz, P. *Appl. Phys. A* **1997**, *63*, 207.
(29) Palik, E. D. *Handbook of Optical Constants of Solids*; Academic: New York, 1985.

NL070653E